BIOCHEMISTRY
including biophysical chemistry & molecular biology
Article

Biochemistry **2009,** *48,* 6963–6974 6963
DOI: 10.1021/bi900152k

Vitamin K3 Disrupts the Microtubule Networks by Binding to Tubulin: A Novel Mechanism of Its Antiproliferative Activity†

Bipul R. Acharya, Diptiman Choudhury, Amlan Das, and Gopal Chakrabarti*

Department of Biotechnology and Dr. B. C. Guha Centre for Genetic Engineering and Biotechnology, University of Calcutta, 35 Ballygunge Circular Road Kolkata, WB 700019, India

Received January 30, 2009; Revised Manuscript Received May 11, 2009

ABSTRACT: Vitamin K3 (2-methyl-1,4-naphthoquinone), also known as menadione, is the synthetic precursor of all the naturally occurring vitamin K in the body. Vitamin K is necessary for the production of prothrombin and five other blood-clotting factors in humans. We have examined the effects of menadione on cellular microtubules ex vivo as well as its binding with purified tubulin and microtubules in vitro. Cell viability experiments using human cervical epithelial cancer cells (HeLa) and human oral epithelial cancer cells (KB) indicated that the IC_{50} values for menadione are 25.6 ± 0.6 and 64.3 ± 0.36 μM, respectively, in those cells. Mendione arrests HeLa cells in mitosis. Immunofluorescence studies using an anti-α-tubulin antibody showed a significant irreversible depolymeriztion of the interphase microtubule network and spindle microtubule in a dose-dependent manner. In vitro polymerization of purified tubulin into microtubules is inhibited by menadione with an IC_{50} value of 47 ± 0.65 μM. The binding of menadione with tubulin was studied using menadione fluorescence and intrinsic tryptophan fluorescence of tubulin. Binding of menadione to tubulin is slow, taking 35 min for equilibration at 25 °C. The association reaction kinetics is biphasic in nature, and the association rate constants for fast and slow phases are 189.12 ± 17 and 32.44 ± 21 M^{-1} s^{-1} at 25 °C, respectively. The stoichiometry of menadione binding to tubulin is 1:1 (molar ratio) with a dissociation constant from 2.44 ± 0.34 to 3.65 ± 0.25 μM at 25 °C. Menadione competes for the colchicine binding site with a K_i of 2.5 μM as determined from a modified Dixon plot. The obtained data suggested that menadione binds at the colchicine binding site to tubulin. Thus, we can conclude one novel mechanism of inhibition of cancer cell proliferation by menadione is through tubulin binding.

Vitamin K is an essential vitamin that was discovered as a fat-soluble anti-hemorrhagic agent (*1*). The K vitamins act as cofactors during post-translation modification at specific glutamate residues of the blood-clotting proteins, factors II, VII, IX, X, protein C, and protein S, which are active forms of clotting factors (*1*−*4*). Vitamin K consists of a family of structurally similar fat-soluble 2-methyl-1,4-naphthoquinones, including phylloquinone (vitamin K1), menaquinone (vitamin K2), and menadione (vitamin K3). All members of the vitamin K family possess an identical naphthoquinone skeleton with various side chains that distinguish them. Vitamin K1 is found in many higher plants as well as algae, with the highest concentrations found in green leafy vegetables (*5*). Vitamin K2 also occurs naturally but is not produced by plants. It is produced by a vast array of intestinal bacteria (*6*). Vitamin K3 (menadione) is not considered a natural vitamin K, but rather a synthetic analogue that acts as a provitamin, and the pharmacological dosages of phylloquinone and menaquinones (menaquinone-4 and -7) are catabolized to release menadione; only upon oral administration of vitamin K had ∼5−25% of the ingested K vitamins been catabolized to menadione (*7*). It possesses a much simpler structure, with no aliphatic chain prosthetic group at position 3. The antitumor action of vitamin K has been under investigation since 1947 (*8*), and most of the anticancer research of vitamin K has been focused on menadione (*9*). The anticancer activity of menadione has also been demonstrated in a number of studies using both rodent and human cancer cell lines (*10*−*14*). Menadione was effective against multi-drug-resistant leukemia cell lines and parental leukemia cell lines (*15*). Several mechanisms have been proposed in the growth inhibitory and cytotoxic effects of menadione. Historically, the main effect is believed to be due to oxidative stress via redox cycling of the quinone to produce reactive oxygen species (*16*), while a lower concentration of menadione induces apoptosis by a nonoxidative mechanism (*17*). In hepatocytes, menadione increases the level of $p21^{Cip1}$, which induces the cell cycle to G0/G1 arrest (*18*, *19*), but it was also reported that vitamin K3 induces G2/M arrest by inhibition of formation of the cyclinB−cdk1 complex in hepatic cancer cells (*20*).

†The work was supported by grants from CSIR, Government of India [37(1216)/05/EMR-II], and BRNS/DAE, Government of India (2006/37/21/BRNS), to G.C. D.C. is supported by a fellowship from BRNS/DAE, and A.D. is supported by a fellowship from the University of Calcutta.

*To whom correspondence should be addressed: Department of Biotechnology and Dr. B. C. Guha Centre for Genetic Engineering and Biotechnology, University of Calcutta, 35 Ballygunge Circular Road Kolkata, WB 700019, India. Telephone: 91-33-2461-5445. Fax: 91-33-2461-4849. E-mail: gcbcg@caluniv.ac.in.

Published on Web 06/15/2009

Microtubules are major structural components of the cytoskeleton of the cell and play important roles in cell motility, intracellular transport, mitosis, and many other cellular processes (*21*−*25*). Highly dynamic microtubules are among the most successful targets for anticancer therapy that inhibit mitosis in mammalian cells by interfering with the rapid dynamics of the spindle microtubules, which are required for normal mitotic progression (*26*). They are dynamic polymers composed of α- and β-tubulin heterodimer. Drugs which bind to the tubulin−microtubule system alter its dynamics in two different ways, either by stabilizing the polymer structure of microtubules like paclitaxel or by inhibiting the polymerization of tubulin into microtubules (*26*−*33*). There are two characterized drug-binding sites in tubulin that inhibit microtubule polymerization. One is the colchicine binding site in α- and β-tubulin interphase, where drugs such as colchicine itself, podophyllotoxin, combreastatin, and curacin A are thought to bind (*26*−*30*). The second is the Vinca binding site, also thought to be in β-tubulin, where the Vinca alkaloids, cryptophycins, and maytansinoids bind (*31*).

Menadione blocks mitosis and inhibits cell proliferation, but whether it has any effect on microtubule dynamics has not been determined. In this study, we examined the binding activity of menadione with tubulin and microtubules. We found that in vitro menadione binds to tubulin at the colchicine binding site and inhibits microtubule polymerization. Menadione binding to tubulin enhances menadione fluorescence and quenches the tryptophan fluorescence of tubulin. Menadione exhibits cytotoxicity in human cervical carcinoma cells (HeLa) and human oropharyngeal carcinoma cells (KB) under ex vivo conditions. We also found that in ex vivo perturbation of interphase and spindle microtubules in human cervical carcinoma cells (HeLa) by menadione, it induces G2/M arrest in the HeLa cell cycle. The results indicate a novel mechanism of cell proliferation inhibition and mitotic block by menadione, and it could be beneficial for the development of potential anticancer agents.

EXPERIMENTAL PROCEDURES

Materials. Nutrient mixture Dulbecco's minimal essential medium (supplemented with 1 mM L-glutamine), fetal bovine serum, penicillin-streptomycin, and amphotericin B were purchased from HyClone. Trypsin-Versene was purchased from Cambrex Bioscience. Menadione (vitamin K3), phylloquinone (vitamin K1), DAPI,[1] anti-mouse monoclonal anti-α-tubulin antibody (raised in mice), anti-mouse rhodamine-conjugated IgG antibody, guanosine 5′-triphosphate (GTP), PIPES, $MgCl_2$, and EGTA were purchased from Sigma. The annexin V-FITC apoptosis detection kit was obtained from BD Biosciences (San Diego, CA). The Bradford protein estimation kit was from Genei. All other chemicals and reagents were of analytical grade and were purchased from Sisco Research Laboratories.

Purification of Tubulin from Goat Brain. Tubulin was isolated from goat brain via two cycles of temperature-dependent assembly and disassembly in PEM buffer containing 50 mM PIPES, 1 mM EGTA, and 0.5 mM $MgCl_2$ (pH 6.9) in the presence of 1 mM GTP, followed by two more cycles in 1 M glutamate buffer (*34*). Aliquots were flash-frozen in liquid nitrogen and stored at −70 °C. The protein concentration was estimated by the method of Bradford (*35*) using bovine serum albumin as the standard.

Preparation of the Menadione Solution. The stock solution of menadione was prepared by adding dry powder of menadione to 100% DMSO. The concentration was determined using the molar extinction coefficient of 3100 M^{-1} cm^{-1} at 340 nm in ethanol (*39*). All the experiments were conducted making the secondary solution in PEM buffer where the final DMSO concentration is less than 1%.

Cell Culture. Human cervical carcinoma cells (HeLa) and human oropharyngeal carcinoma cells (KB) were maintained in nutrient mixture DMEM supplemented with 1 mM L-glutamine, 10% fetal bovine serum, 50 μg/mL penicillin, 50 μg/mL streptomycin, and 2.5 μg/mL amphotericin B. Cells were cultured at 37 °C in a humidified atmosphere containing 5% CO_2. Cells were grown in tissue culture flasks until they were 80% confluent before trypsinization with 1× trypsin-versene and splitting. The morphology of normal and treated cells was observed with an Olympus model CKX41 inverted microscope.

Cell Proliferation Inhibition Assay (MTT Assay). Cultured HeLa and KB cells were plated in 96-well culture plates (1×10^4 cells per well). After incubation for 24 h, the cells were treated with menadione (0, 5, 10, 20, 30, and 50 μM) for 12 h. MTT (5 mg/mL) was dissolved in PBS and filter sterilized, and then 20 μL of the prepared solution was added to each well. This was incubated until a purple precipitate was visible. Subsequently, 100 μL of Triton-X was added and incubated in the well in the dark for 2 h at room temperature. The absorbance was measured on an ELISA reader (MultiskanEX, Lab systems, Helsinki, Finland) at a test wavelength of 570 nm and a reference wavelength of 650 nm. Data were calculated as the percentage of inhibition by the following formula:

$$\%\text{inhibition} = [100 - (A_t/A_s) \times 100] \quad (1)$$

where A_t and A_s are the absorbance of the test substances and solvent control, respectively (*28*).

Flow Cytometric Analysis for Apoptotic and Necrotic Cells. To examine the presence of apoptosis and necrosis induced by menadione, 1×10^5 HeLa cells were cultured with different concentrations of menadione for 24 h. As a control, HeLa cells were cultured without vitamin K. Approximately 1×10^5 cells were then stained for 15 min at room temperature in the dark with fluorescein isothiocyanate (FITC)-conjugated annexin V (1 μg/mL) and PI (0.5 μg/mL) in a Ca^{2+}-enriched binding buffer and analyzed by a two-color flow cytometric assay. Annexin V and PI emissions were detected in the FL1 and FL2 channels of a FACSCalibur flow cytometer, using emission filters at 525 and 575 nm, respectively. The annexin V-negative/PI-negative population was regarded as normal and healthy, while annexin V-positive/PI-negative and annexin V-positive/PI-positive cells were taken as a measure of apoptosis and necrosis, respectively. Apoptosis analysis was performed using the Becton Dickinson FACScan instrument, and the data were analyzed using CellQuest from Becton Dickinson.

Cell Cycle Analysis by Flow Cytometry. HeLa cells were seeded at a density of 3×10^4 cells/mL. Menadione (25 μM) was added and was incubated for 18 h. After 18 h, the cells were harvested, fixed in ice chilled methanol for at least 30 min at 4 °C, and incubated for 4 h at 37 °C in a PBS solution containing 1 mg/mL RNase A. Cell cycle analysis was performed using the Becton

[1]Abbreviations: PIPES, 1,4-piperazinediethanesulfonic acid; EGTA, ethylene bis(oxyethylenenitrilo) tetraacetic acid; GTP, guanosine 5′-triphosphate; DTNB, 5,5′-dithiobis(2-nitrobenzoic acid); DAPI, 4′,6-diamidino-2-phenylindole; AC, 2-methoxy-5-(2′,3′,4′-trimethoxyphenyl)tropone; PI, propidium iodide; FITC, fluorescein isothiocyanate; MTT, 3-(4,5-dimethylthiazolyl-2)-2,5-diphenyltetrazolium bromide.

Dickinson FACScan instrument, and the data were analyzed using CellQuest from Becton Dickinson.

Mitotic Progression. To evaluate mitotic indices, HeLa cells were plated at a density of 3×10^4 cells/mL. After 48 h, cells were incubated in the absence or presence of menadione over a range of concentrations (10−25 μM) for 20 h. Media were collected, and cells were rinsed with PBS twice, detached by trypsinization, and added back to the media to ensure that floating and poorly attached mitotic cells were included in the analysis. Cells were fixed with 10% formalin for 30 min, permeabilized in ice-cold methanol for 10 min, and stained with 4′,6′-diamidino-2-phenylindole (DAPI) (1 μg/mL) to visualize nuclei. Mitotic indices were determined with a Ziess LSM 510 Meta confocal microscope. Results are the means and standard error of the mean (SEM) of three experiments in each of which 500 cells were counted at each concentration (*32*).

Sample Preparation for Confocal Microscopy. Human cervical epithelial carcinoma cells (HeLa) were seeded on coverslips at a density of 1×10^5 cells/mL and incubated in the presence of different doses of menadione (0−50 μM) for 18 h. Subsequently, cells were washed twice with PBS washing buffer, and cells were fixed with 2% paraformaldehyde. Cell permeable solution (0.1% sodium citrate and 0.1% Triton) was added, and cells were incubated at room temperature for 1 h. Nonspecific binding sites were blocked by incubating the cells with 5% BSA. Cells were then incubated with anti-mouse monoclonal anti-α-tubulin antibody (1:200 dilution) followed by anti-mouse rhodamine-conjugated IgG antibody (1:150 dilutions) and DAPI (1 μg/mL). After incubation, cells were washed with PBS and viewed under a Ziess LSM 510 Meta confocal microscope.

Western Blot Analysis. The cellular tubulin polymerization was quantified by a modified method which was originally described by Minotti et al. (*33*). Cultured HeLa cells were treated with different concentrations of menadione (25−50 μM) and colchicine (3 μM) for 18 h. Then the cells were washed twice with PBS and harvested by trypsinization. Cells were lysed at 37 °C for 5 min in the dark with 100 μL of hypotonic lysis buffer [1 mM $MgCl_2$, 2 mM EGTA, 0.5% NP-40, 20 μg/mL aprotinin, 20 μg/mL leupeptin, 1 mM orthovanadate, 2 mM PMSF, and 20 mM Tris-HCl (pH 6.8)]. After a brief but vigorous vortex, the samples were centrifuged at 14000 rpm (21000*g*) for 10 min. The 100 μL supernatants containing soluble (cytosolic) tubulin were separated from the pellets containing polymerized (cytoskeletal) tubulin. The pellets were resuspended in 100 μL of lysis buffer. The total concentrations of proteins in the soluble fraction and pellet fraction were estimated separately by the Bradford method. Equal amounts (50 μg) of each sample were added with SDS−polyacrylamide gel electrophoresis sample buffer and run in a 10% SDS−polyacrylamide gel. The sample was then analyzed by Western blotting and probed with the antibody against α-tubulin (1:1000 dilutions).

Microtubule Polymerization. Tubulin (1.2 mg/mL) was mixed with different concentrations of menadione (0−80 μM) and incubated for 30 min at 25 °C. The polymerization reaction was initiated by incubating the tubulin−menadione complex in polymerization buffer [1 mM $MgSO_4$, 1 mM EGTA, and 1.0 M monosodium glutamate (pH 6.8)] at 37 °C just after addition of 1 mM GTP to the assembly. The rate and the extent of the polymerization reaction were monitored by light scattering at 350 nm using a Jasco V-630 spectrophotometer (*37*).

Spectral Measurements. All fluorescence measurements were performed using a Hitachi model F-3010 fluorescence spectrophotometer equipped with a constant-temperature water circulating bath. A 1 cm path length quartz cuvette was used for all fluorescence measurements. Fluorescence data were corrected for the inner filter effect according to the equation of Lakowicz (*38*).

$$F = F_{obs}\ \text{antilog}[(A_{ex}+A_{em})/2] \quad (2)$$

where A_{ex} is the absorbance at the excitation wavelength and A_{em} is the absorbance at the emission wavelength (*38*). All absorbance measurements were performed in a JASCO V-630 UV−visible spectrophotometer using a quartz cuvette with a path length of 1 cm.

Binding Study by Fluorometric Titration. Association Kinetics. The kinetics of the association of menadione with tubulin was measured under pseudo-first-order conditions, where the ligand was present in a large excess using a Hitachi model F-3010 fluorescence spectrophotometer. Concentrations of menadione were 20, 30, and 40 μM, whereas the tubulin concentration was 1 μM (*39*). The ligand was added to the tubulin solution, and emission at 336 nm was measured upon excitation at 295 nm (excitation and emission slits were 5 and 10 nm, respectively). The quenching data were analyzed according using Lambier and Engelborgh's method (*39*, *40*) after correction for the inner filter effect.

$$F = Ae^{-k_1 t} + Be^{-k_2 t} + C \quad (3)$$

where F is the fluorescence of the ligand−tubulin complex at time t, A and B are the amplitudes for the fast and slow phases, respectively, k_1 and k_2 are the pseudo-first-order rate constants for these fast and slow phases, respectively, and C is an integration constant. The data were analyzed with Microcal Origin version 7.0. The apparent second-order rate constant (k_{on}) was obtained by dividing the observed rate constant for the fast phase (k_1) and the slow phase (k_2) by the ligand concentration.

Enhancement of the Fluorescence of the Ligand upon Its Binding to Tubulin. The increased menadione fluorescence at 418 nm upon its binding to tubulin was observed. Initial experiments showed that the increase in menadione fluorescence upon its binding to tubulin attained saturation after incubation for 20 min at 25 °C. Menadione (5 μM) showed its fluorescence enhancement upon incubation with 0−25 μM tubulin in 25 mM PIPES (pH 6.8), 3 mM $MgSO_4$, and 1 mM EGTA (buffer A) at 25 °C for 30 min. The excitation and emission wavelengths were 340 and 418 nm, respectively. The apparent increases in the fluorescence values in the presence of varying concentrations of tubulin corrected for the inner filter effect were determined according to eq 2. Binding parameters were determined using the relationship $\Delta F_{max}/\Delta(F - F_o) = K_d/[\text{free menadione}] + 1$, where K_d corresponds to the dissociation constant, $\Delta(F - F_o)$ is the change in fluorescence intensity when tubulin and menadione are in equilibrium, and ΔF_{max} is the value of maximum fluorescence change when tubulin is completely liganded with menadione. ΔF_{max} was calculated by plotting $1/\Delta(F - F_o)$ versus $1/[\text{menadione}]$, using the total ligand concentration as a first estimate of free ligand concentration, and the calculation was repeated until there was no change in the value of the ΔF_{max} (*40*, *41*).

Job Plot. The stoichiometry of binding was determined using the method of continuous variation (*42*). Several mixtures of tubulin and menadione were prepared by continuously varying concentrations of tubulin and menadione in the mixture, keeping the total concentration of menadione with tubulin constant at 5 μM. Reaction mixtures were incubated for 30 min at 25 °C, and

the fluorescence measurements were recorded using 340 nm as an excitation wavelength.

Equilibrium Constant. Tubulin (2 μM) was incubated with varying concentrations of menadione (0−30 μM) at 25 °C for 30 min. The fluorescence measurements were performed using 295 nm as the excitation wavelength, and the wavelength scan was conducted between 310 and 400 nm. We selected 295 nm as the excitation wavelength to specifically excite the tubulin tryptophan residues. When excited at 295 nm, tubulin displayed a typical emission spectrum with a maximum at 335 nm, and menadione reduced the intrinsic fluorescence of tubulin. The apparent decreases in the fluorescence values in the presence of varying concentrations of menadione were corrected for the inner filter effect according to eq 1. The fraction of binding sites (X) occupied by menadione was determined using the equation $X = (F_o - F)/F_{max}$, where F_o is the fluorescence intensity of tubulin in the absence of menadione, F is the corrected fluorescence intensity of tubulin in the presence of menadione, and F_{max} is calculated from the plot of $1/(F_o - F)$ versus 1/[menadione] and extrapolating 1/[menadione] to zero. The dissociation constant (K_d) was determined using the relationship $F_{max}/(F_o - F) = 1 + K_d/L_f$, where L_f represents the free menadione concentration, and $L_f = C - X$[Y], where C is total concentration of menadione and [Y] is the molar concentration of ligand binding sites, using a stoichiometry of 1:1 as determined from the Job plot.

Effect of Menadione on the Formation of the Colchicine−Tubulin Complex. Colchicine binding to tubulin was assessed by measuring the fluorescence of the tubulin−colchicine complex (*43*). A modified Dixon plot for the menadione was obtained using colchicine as a competitive inhibitor. The reaction mixtures containing tubulin (3 μM) and varied concentrations of colchicine (5−15 μM) and menadione (0−75 μM) were incubated at 37 °C for 45 min. The reciprocal of the fluorescence intensity of the colchicine tubulin complex at 430 nm was plotted versus the concentration of the menadione, while the excitation wavelength was 380 nm. The resulting Dixon plot gave an approximate K_i value for the menadione (*44*).

Statistical Analysis. Data are presented as the mean of at least three independent experiments along with SEM. Statistical analysis of data was conducted by a Student's t test, by using MS Excel, and two measurements were statistically significant if the corresponding p value was <0.05.

RESULTS

Menadione Inhibits Proliferation of KB and HeLa Cells. Menadione inhibited proliferation of human cervical carcinoma (HeLa) and human oropharyngeal carcinoma (KB) cell lines in a concentration-dependent manner as measured by MTT assay (Figure 1B,C) (explained in Experimental Procedures). Maximal proliferation inhibition in the case of HeLa cells was observed at 24 h with 75 μM menadione, which inhibited 92.35% proliferation with the calculated IC_{50} value of 25.6 ± 0.6 μM, whereas in KB cells, the maximum proliferation inhibition was observed at 24 h with 100 μM menadione, which inhibited 83.70% proliferation. The IC_{50} value of in KB cells is 64.3 ± 0.36 μM.

Menadione Induces Apoptosis in HeLa Cells. To quantify the mode of cell death (apoptosis or necrosis) induced by menadione, HeLa cells were incubated in the absence and presence of 10, 25, and 50 μM menadione for 24 h. Cells were then stained with annexin V and PI and analyzed by flow cytometry. Annexin V-positive/PI-negative cells were taken as a measure of apoptosis. As shown in Figure 2A, vitamin K3 induced apoptosis of HeLa cells. The ratios of apoptotic cells were 24.57, 44.09, and 66.45% when the cells were treated with 10, 25, and 50 μM menadione, respectively, while it was only 0.51% when the cells were cultured without menadione. The increased fluorescence of the FITC-annexin V-positive apoptotic cells was observed by confocal microscope with respect to nonapoptotic control cells (Figure 2B). These results clearly indicated that menadione induces apoptosis in HeLa cells.

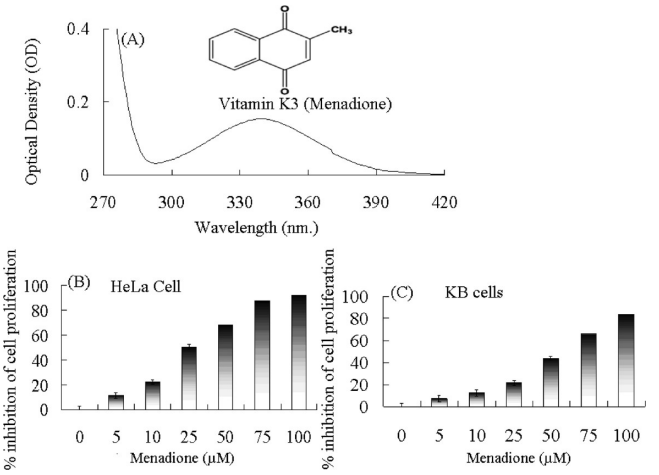

FIGURE 1: (A) Absorption spectrum of 50 μM menadione. The inset shows the chemical structure of menadione (2-methyl-1,4-naphthoquinone). (B and C) Concentration-dependent inhibition of cell proliferation (MTT assay). Results of the MTT assay of 0−100 μM menadione-treated HeLa cells (B) and KB cells (C). Details of the experiment are given in Experimental Procedures.

Menadione Induces G2/M Cell Cycle Arrest of HeLa Cells. To examine the mechanism responsible for menadione-mediated cell growth inhibition, cell cycle distribution was analyzed using a flow cytometric method as shown in Figure 3A. The ratios of untreated cells in G0/G1, S, and G2/M phases of the cell cycle were 41.3, 7.37, and 18.16%, respectively, and in the presence of 0.5 μM paclitaxel (used as a positive control), the ratios were 10.59, 11.79, and 44.82%, respectively. In the presence of 25 μM menadione, the ratios of G0/G1, S, and G2/M became 12.89, 7.76, and 50.34%, respectively, resulting in a clear increase in the percentage of cells in the G2/M phase compared to that of untreated cells, and are comparable with those of paclitaxel-treated cells, and this indicates that menadione arrests the HeLa cell cycle at the G2/M phase.

Determination of the Mitotic Index of Menadione-Treated HeLa Cells. To further determine whether menadione inhibited cell cycle progression in mitosis, the mitotic indices of normal and menadione-treated HeLa cells were calculated by confocal microscopy after fixing and staining of cells (details in Experimental Procedures). In the absence of menadione, 4.5% of HeLa cells were in mitosis; after the addition of menadione, as cells entered the M phase of the cell cycle, many of them were unable to progress through mitosis, and they began to accumulate in mitosis (Figure 3B,C and Table 1). Many of the cells that were not blocked in mitosis were in an abnormal multinucleate interphase and may have undergone an abortive mitosis and reverted to interphase without successful cytokinesis (Figure 3B). Again, the percentage of cells in mitosis was increased after treatment of HeLa cells with menadione for 18 h in a concentration-dependent manner (Figure 3C). In the presence 10 and 25 μM menadione, 22 and 42% of total cells were in mitosis,

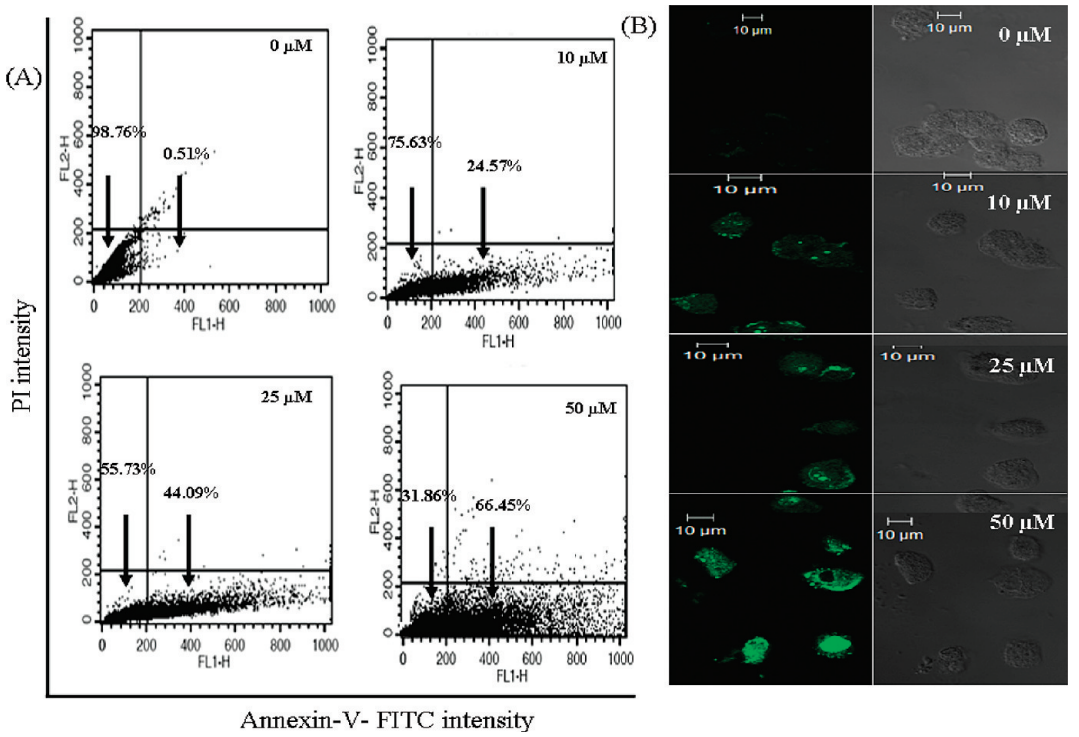

FIGURE 2: Menadione induces apoptosis in HeLa cells. (A) Annexin V-FITC/PI assay showing that menadione induces apoptosis in HeLa cells. Untreated cells and cells treated with 10, 25, and 50 μM menadione were harvested following exposure for 18 h and stained with annexin V-FITC and PI. The percentage of early apoptotic cells in the bottom right quadrant (annexin V-FITC positive/PI-negative cells) as well as late apoptotic cells located in the top right quadrant (annexin V-FITC-positive/PI-negative cells). (B) Immunofluorescence study of annexin V-FITC-positive apoptotic HeLa cells. The left panels show the control cells (annexin V-FITC-negative) and menadione-treated cells (annexin V-FITC-positive), and the right panels show the corresponding phase contrast images of the cells.

respectively. Table 1 also lists the distribution of the cell in different mitotic phases, where it is evident that cells are mainly blocked on the prophase/prometaphase and metaphase, whereas the arrest of anaphase and telophase is comparatively weaker. Together, all data indicated that menadione arrests HeLa cells in mitosis.

Disruption of the Interphase Microtubule Network of HeLa Cells by Menadione. Because the tubulin−microtubule system has a major role in the maintenance of cellular integrity and because menadione induced apoptosis and arrest of mitosis in HeLa cells, we were interested to know whether menadione targets the microtubule network in cultured HeLa cells. This was examined by confocal microscopy, and the results are shown in Figure 4A−F. Control HeLa cells exhibited typical interphase microtubule organization (Figure 4A,B). No effect of menadione on the interphase microtubule network was apparent at menadione concentrations below 10 μM. However, at relatively higher menadione concentrations (25 μM), a significant reduction in microtubule density occurred (Figure 4C,D). A substantial reduction in the number of microtubules at the periphery of the cells was apparent, and the central networks were disorganized. Menadione depolymerized interphase microtubules greatly in HeLa cells at 50 μM (Figure 4E,F).

Menadione Perturbs Mitotic Spindle Organization. In untreated cells, normal bipolar spindles were observed with chromosomes congressed in the form of compact metaphase plates. Effects of menadione on the spindle microtubules of HeLa cells are shown in Figure 4G−L. Menadione depolymerized spindle microtubules in a concentration-dependent manner. In the presence of 10 and 25 μM menadione, the chromosomes were unable to organize in the metaphase plate. These results indicated that menadione may inhibit microtubule polymerization and reduce the microtubule density in the cytoplasm.

Menadione Reduces the Polymerized Microtubule Mass in HeLa Cells. To quantify the effect of menadione on microtubule mass in HeLa cells, Western blot analyses were performed for the soluble tubulin and the assembled tubulin of HeLa cells after treatment with menadione against anti-α-tubulin antibody. As shown in Figure 4M, the level of soluble tubulin in menadione-treated cells was decreased compared to that in control cells (untreated cells). Cells treated with 25 and 50 μM menadione also showed a decreased amount of the polymer form of tubulin (Figure 4M, lanes 2 and 3), while the total amount of tubulin remains unchanged. These results show a pattern similar to that of colchicine, a microtubule-depolymerizing agent (positive control, lane 4, Figure 4M).

Menadione Irreversibly Depolymerizes Microtubules in HeLa Cells. Drugs like colcemid depolymerize microtubules reversibly; on removal of the drug, the formation of new microtubules or repolymerization of microtubules takes place in cells (*45*). To determine whether menadione had the same effect, we incubated the HeLa cells with the IC_{50} concentration of menadione (25 μM) for 18 h, then washed off the menadione-containing medium, washed the cells thrice with fresh PBS, and finally replaced the fresh medium and placed the cells in a 37 °C incubator for different periods of time (0−24 h). Finally, we viewed them under a confocal microscope, and no significant repolymerization of the microtubule network was observed (Figure 5), which suggests the irreversible pattern of damage of the microtubule network by menadiones like cryptophycin and sanguinarin (*46*, *47*).

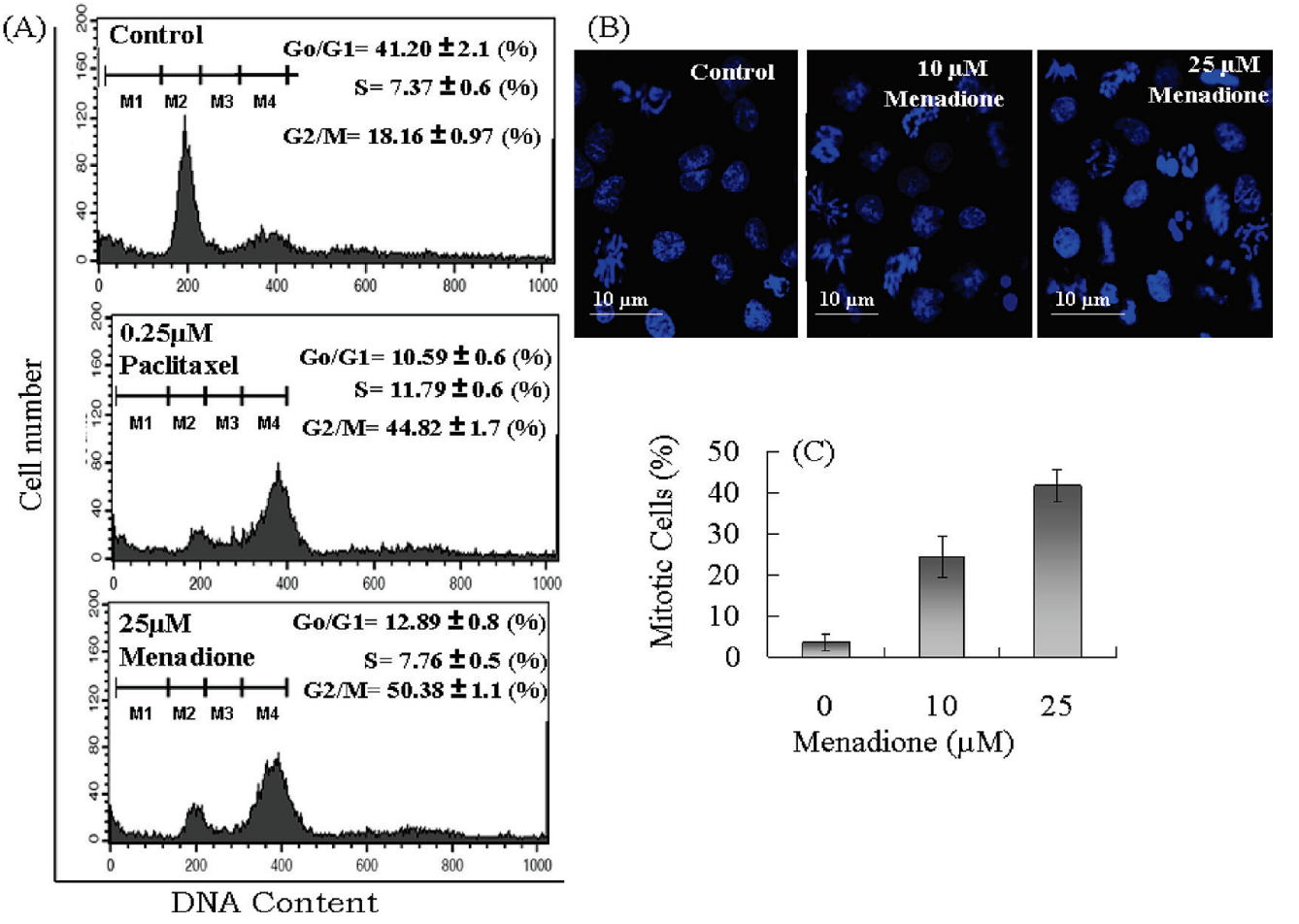

FIGURE 3: (A) Flow cytometric analysis of the cell cycle distribution of HeLa cells treated with menadione. Cultured HeLa cells were treated with 25 and 0.25 μM paclitaxel separately for 18 h. Cell cycle analysis was conducted using BD FACScaliber, and data were analyzed with CellQuest (Becton Dickinson). Here M1, M2, M3, and M4 indicate sub-G0, G0/G1, S, and G2/M phase, respectively. (B) Effect of menadione on chromosomes of HeLa cells. Cultured HeLa cells were fixed and stained with DAPI (1 μg/mL) for the observation of chromosomes in different stages of mitosis; also, normal and abnormal interphase nuclei are observed in the absence (control cells) and in the presence of menadione (10−25 μM) for 18 h. Details of the experiment are given in Experimental Procedures. (C) Effect of menadione on mitosis in HeLa cells. Cultured HeLa cells were treated with 0−25 μM menadione for 18 h. Cells were then fixed and stained with DAPI (1 μg/mL). Mitotic indices were determined by counting interphase and mitotic cells at 40× magnification using a confocal microscope. At least 1000 cells per data point were counted. Data are presented as means ± SEM ($p < 0.01$) where $n = 3$.

Table 1: Distribution of HeLa Cells in Different Mitotic Phases after Treatment with Menadione[a]

menadione (μM)	inter (% of cells)	pro/prometa (% of cells)	meta (% of cells)	ana/telo (% of cells)
0	95.5 ± 0.67	2.3 ± 0.31	1.2 ± 0.04	0.97 ± 0.33
20	76.3 ± 0.42	13.21 ± 0.76	7.84 ± 0.83	1.1 ± 2.3
23	61.23 ± 2.7	18.64 ± 0.97	20.41 ± 0.72	2.3 ± 1.4

[a] Cells were grown on collagen-coated coverslips and treated with 0, 10, and 25 μM menadione for 18 h. Cells were then stained with DAPI (1 μg/mL) and counted for distribution in various phases of the cell cycle. At least 1500 cells on each slide were counted. Values are means ± SEM ($p < 0.03$) where $n = 3$. Abbreviations: inter, interphase; pro, prophase; prometa, prometaphase; meta, metaphase; ana, anaphase; telo, telophase.

Menadione Suppresses Reassembly of Cold Depolymerized Microtubules in HeLa Cells. Microtubules were depolymerized when the HeLa cells were incubated at 4 °C for 3 h (until the cell appeared round), as shown in Figure 6B. Subsequently, the kinetics of the reassembly of the microtubules in live HeLa cells was monitored by incubating the cells with warm medium containing different concentrations of menadione at 37 °C. In control cells, depolymerized interphase microtubules reassembled to form a normal microtubule network within 60 min of incubation at 37 °C (Figure 6C). In the presence of 10, 25, and 50 μM menadione, microtubules failed to reassemble even after incubation for 60 min at 37 °C (Figure 6C−E). In the absence of menadione, spindle microtubules assembled fast and formed normal mitotic spindles (Figure 6I). In the presence of 10, 25, and 50 μM menadione, spindle reassembly was hindered (Figure 6J,K) and it was not detectable in cells treated with 50 μM menadione (Figure 6M).

Inhibition of Microtubule Polymerization by Menadione in Vitro. Since we have already noticed that menadione affects the cellular architecture of human cervical carcinoma (HeLa) cells by perturbing the intercellular microtubular network, we examined the effect of menadione on microtubule polymerization

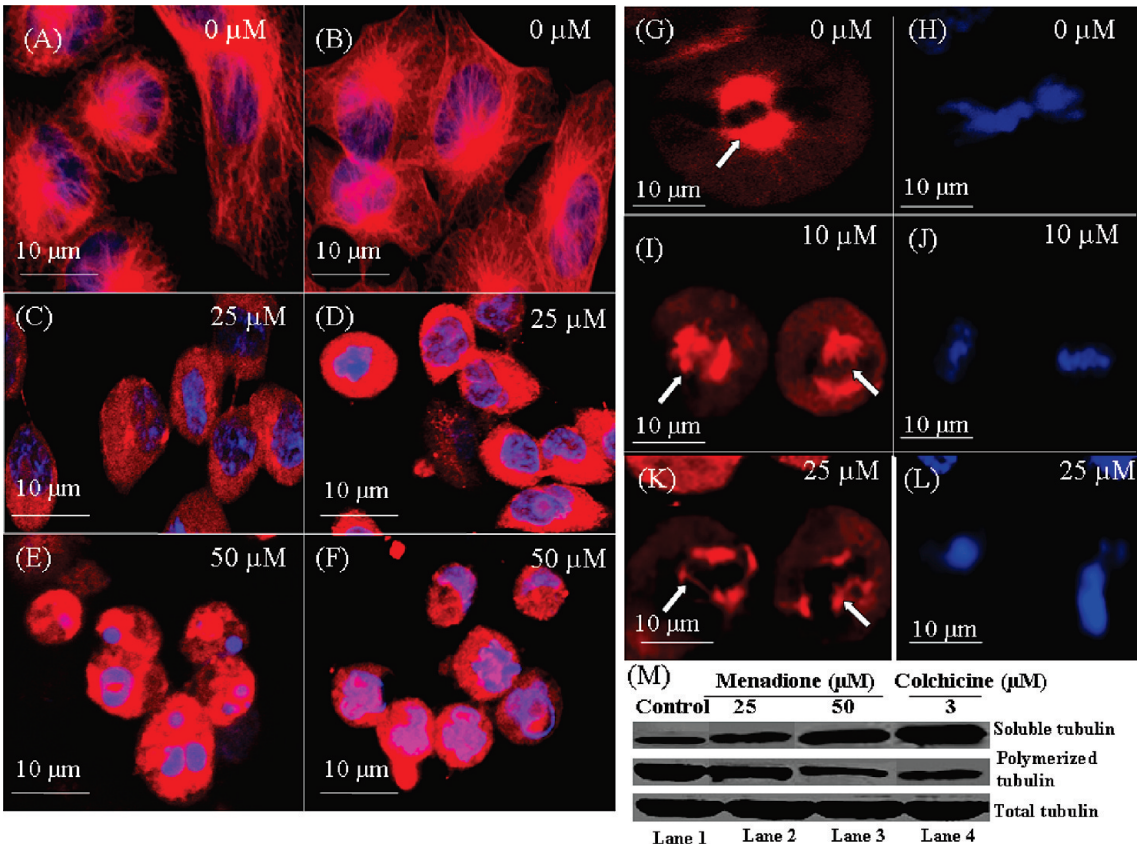

FIGURE 4: (A−F) Effects of menadione on the interphase microtubules of HeLa cells. Cells were incubated with 0, 10, 25, and 50 μM menadione for 18 h. Microtubules tagged with rhodamine (red) and nuclei tagged with DAPI (blue) were visualized with a confocal microscope as described in Experimental Procedures. (G−L) Effects of menadione on spindle microtubule and chromosome organization of the HeLa cells. HeLa cells were grown in the absence and presence of 10 and 25 μM menadione for 18 h. The spindle microtubule was tagged with rhodamine (red), and the chromosomal arrangement was tagged with DAPI (blue). Details of the experiment are given in Experimental Procedures. (M) Effect of menadione on tubulin polymerization in HeLa cells. HeLa cells were treated with 0, 25, and 50 μM menadione over an 18 h period. Cells were lysed with a hypotonic lysis buffer. Following cell lysis, the polymerized and soluble form of tubulins was separated by centrifugation. Western blot analysis was conducted using an antibody against α-tubulin.

using purified tubulin. We first analyzed the ability of menadione to inhibit polymerization of purified tubulin into microtubules in vitro by the light scattering assay (as explained in Experimental Procedures). Purified tubulin (12 μM) was polymerized in the absence or presence of different concentrations of menadione, and the results of such experiments are shown in Figure 7A. Menadione inhibited the rate and extent of tubulin polymerization in a concentration-dependent manner (Figure 7B). For example, the level of inhibition of polymerization was 74% when 80 μM menadione was added. The percentage inhibition of microtubule polymerization was calculated using the absorbance readings in the absence and presence of different concentrations of menadione (Figure 5B), and 50% inhibition of microtubule polymerization (IC_{50}) occurred at a menadione concentration of 47.0 ± 0.65 μM ($p < 0.01$).

Menadione Binding to Tubulin. The binding of menadione to tubulin has been studied by measuring the intrinsic quenching of the tryptophan fluorescence of tubulin. Menadione quenches the intrinsic tryptophan fluorescence of tubulin in a time- and concentration-dependent manner. Addition of 40 μM menadione to tubulin (1 μM) quenches ~76% of the tryptophan fluorescence of tubulin during a 30 min incubation at 25 °C (Figure 8A). The level of quenching was ~17% when menadione was just added to tubulin. The increase in the level of tryptophan quenching with time indicates time-dependent binding at 25 °C which is slow and takes ~30 min to reach completion. Similar results are observed when colchicine is added to tubulin (data not shown). However, menadione did not alter the λ_{max} of the tryptophan emission wavelength of tubulin, suggesting that the binding of menadione did not alter the polarity of the immediate environment of tryptophan residues in tubulin.

The association rate constant for different concentrations of menadione with tubulin was determined by ligand-induced quenching of tubulin fluorescence. Figure 8A shows the kinetic profile for the binding of menadione to tubulin under pseudo-first-order conditions for 30 min at 25 °C. The quenching data were analyzed using a biexponential equation as explained in Experimental Procedures (Figure 8B). The apparent second-order rate constant for the first association phase calculated from the equation as shown in Experimental Procedures has been found to be 189.12 ± 17 M^{-1} s^{-1} at 25 °C, whereas the rate constant for the slow association phase calculated from the same equation is 32.44 ± 21 M^{-1} s^{-1} taking the average of nine consecutive experimental data analyses at three different concentrations (20, 30, and 40 μM) of menadione. Under the same experimental condition at 25 °C, we analyzed the fast phase and slow phase association rate constants for association of colchicine with tubulin using the biexponential equation, and the values were 111.35 ± 24 and 72.61 ± 11 M^{-1} s^{-1}, respectively.

The binding of menadione to tubulin was also monitored by enhancement of menadione fluorescence upon binding with tubulin. Menadione has weak fluorescence in neutral aqueous

buffer (Figure 9A), with maxima at 424 nm upon excitation at 340 nm. When menadione was mixed with tubulin in a different molar ratio, the fluorescence intensity of menadione increased markedly (Figure 9A). For example, the fluorescence intensity of 5 μM menadione was increased ≈3-fold in the presence of an equimolar concentration of tubulin; the emission spectrum of the menadione showed a blue shift upon binding to tubulin, and the emission maxima shifted to 418 nm. These results indicated that the polarity of the environment of menadione and its mobility are changed after menadione binds to tubulin. Figure 9B shows the titration curve (menadione fluorescence enhancement) of a constant amount of menadione (5 μM) with various concentrations of tubulin (0−25 μM).

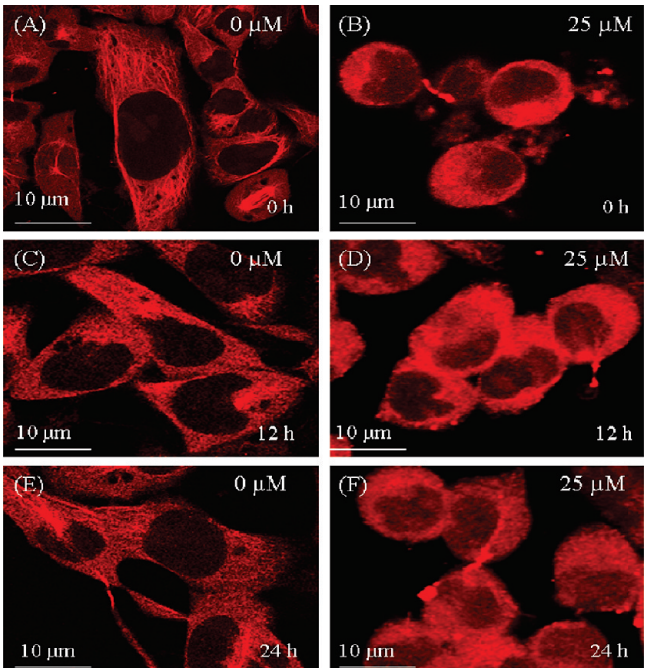

FIGURE 5: Immunofluorescence study showing the irreversible damage pattern of interphase microtubules by menadione. After incubation of HeLa cells with different concentrations of menadione (0−25 μM), the medium was discarded, cells were washed thrice with PBS, fresh medium was added, and after incubation for 0 (A and B), 12 (C and D), and 24 h (E and F) at 37 °C, images were taken with a confocal microscope. Microtubules are tagged with rhodamine (red). Details of the experiment are given in Experimental Procedures.

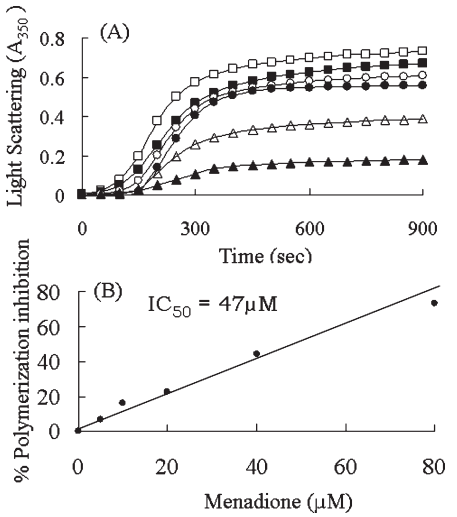

FIGURE 7: Inhibition of microtubule assembly by menadione in vitro. (A) Effect of menadione on microtubule polymerization kinetics assessed by monitoring the increase in light scattering at 350 nm: control (□) and 5 (■), 10 (○), 20 (●), 40 (△), and 80 μM menadione (▲). (B) Inhibition of tubulin polymerization plotted as a function of menadione concentration. Data are representative of three similar experiments.

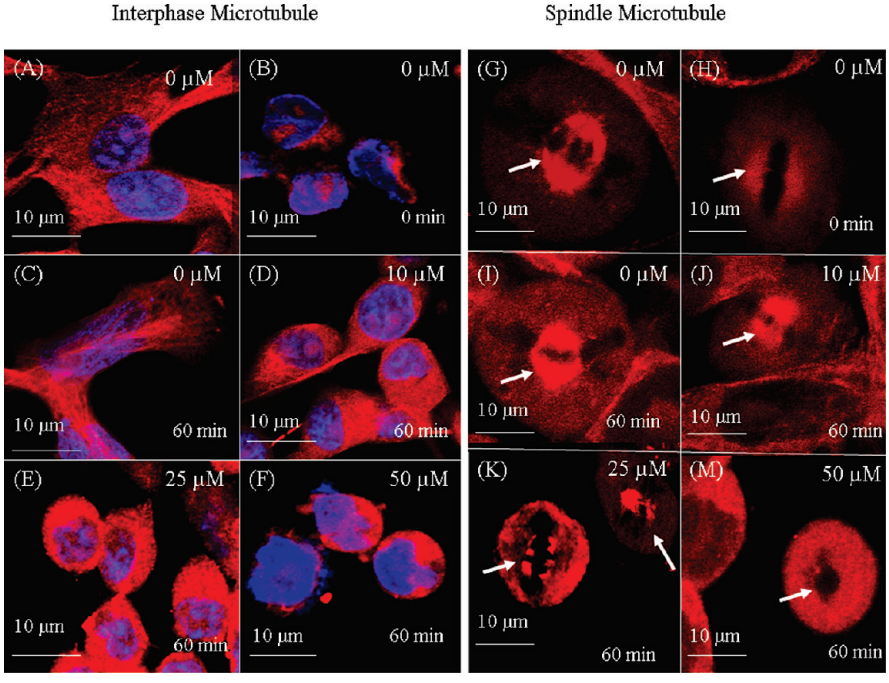

FIGURE 6: Immunofluorescence study of tubulin reassembly in HeLa cells in the presence of menadione after cold depolymerization. Panels A and G show the interphase and spindle microtubule, respectively, before cold treatment. Microtubules of HeLa cells were depolymerized by incubation at 4 °C for 3 h (B and H). Cold media were replaced by warm media containing 0 (C and I), 10 (D and J), 25 (E and K), and 50 μM menadione (F and L) and incubated at 37 °C for 60 min. Microtubules are tagged with rhodamine (red), and nuclei are tagged with DAPI (blue). Details of the experiment are given in Experimental Procedures.

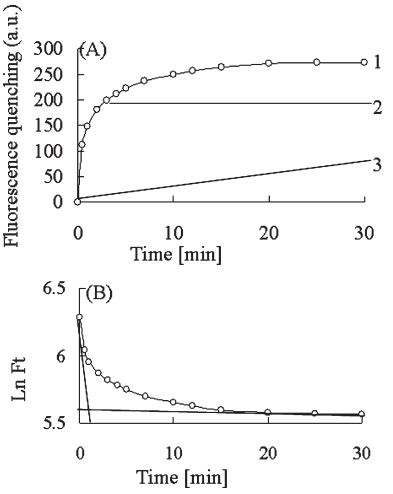

FIGURE 8: Kinetics of binding of menadione to tubulin. (A) Quenching of tryptophan fluorescence of tubulin upon binding of menadione to tubulin. Tubulin (1 μM) in PEM buffer was mixed with 40 μM menadione. The kinetics was followed for 30 min at 25 °C by measuring the intensity of the intrinsic protein fluorescence at 335 nm upon excitation at 295 nm: trace 1, overall quenching of tryptophan fluorescence; trace 2, fast phase; and trace 3, slow phase as determined by the analysis described in Experimental Procedures. (B) Semilogarithmic plot of ln F_t vs time. The biphasic plot obtained was resolved into its component phases as described in Experimental Procedures. The fast and slow phases are shown in traces 2 and 1, respectively. Data are represented as means ± SEM ($p < 0.01$) where $n = 3$.

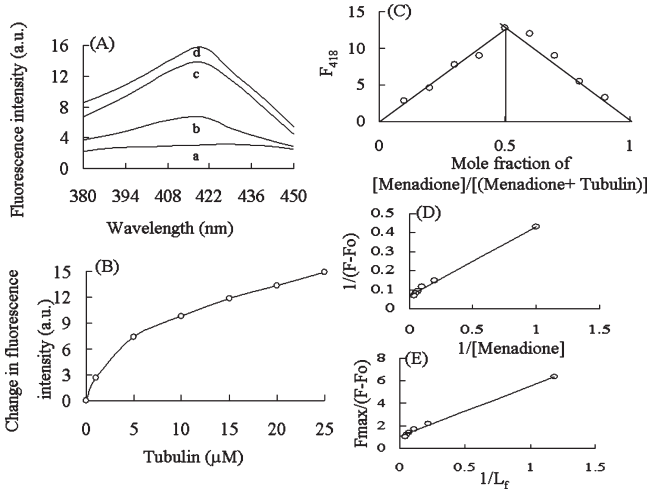

FIGURE 9: Binding of menadione to tubulin was assessed by fluorescence spectroscopy. (A) Graph a shows the fluorescence spectrum of 5 μM menadione in PEM buffer, and graphs b–d show the fluorescence spectrum of 5 μM menadione in the presence of 5, 15, and 25 μM tubulin, respectively. Excitation at 340 nm where the emission maximum is at 418 nm. Spectra were recorded after incubation for 30 min at 25 °C. (B) Titration of 5 μM tubulin with the different concentrations (5–25 μM) of menadione. The excitation wavelength was 340 nm. (C) Job plot for binding of menadione to tubulin. The concentrations of tubulin and menadione were varied continuously while the total concentration of menadione and tubulin was kept constant at 5 μM. The corrected fluorescence intensities at 418 nm were plotted against the mole fractions of menadione. Data are represented as means ± SEM ($p < 0.01$) where $n = 3$. (D) Double-reciprocal plot for binding of menadione to tubulin. F_{max} has been determined from the $1/(F - F_0)$ and 1/[menadione] graph. (E) Linear plot of binding of menadione to tubulin. Data are represented as means ± SEM ($p < 0.01$) where $n = 3$. Data are representative of three identical experiments.

The stoichiometry and the dissociation constant (K_d) of the tubulin–menadione interaction have been estimated by measuring menadione fluorescence enhancement. The stoichiometry of the drug–protein complex was determined using the Job plot. In this plot, concentrations of both tubulin and menadione were varied while the total drug–protein concentration was kept fixed at 5 μM. Results of such experiments are shown in Figure 9C. The stoichiometry of binding calculated by using this method of continuous variation has been found to be 1:1. From the titration curve (Figure 9B) of a constant amount of menadione (5 μM) and various concentrations of tubulin (0–25 μM), the binding data were analyzed as described in Experimental Procedures, and the analysis of the data yielded a linear plot with a dissociation constant of 3.65 ± 0.25 μM (Figure 9D,E). Taken together, these data suggested that menadione binds to tubulin at a single site.

The stoichiometry and the dissociation constant (K_d) of the tubulin–menadione interaction have also been investigated by measuring the effects of menadione on the intrinsic tryptophan fluorescence of tubulin. As shown in Figure 10A, menadione reduced the intrinsic tryptophan fluorescence of tubulin in a concentration-dependent fashion. The stoichiometry of binding calculated by using this method of continuous variation (Job plot) has also been found to be 1:1 (data not shown). The double-reciprocal plot of the binding data (Figure 10B,C) yielded a dissociation constant of 2.44 ± 0.34 μM, which is in excellent agreement with the K_d obtained by the ligand fluorescence titration.

Menadione Binds Tubulin Competitively at the Colchicine Binding Site. Many structurally unrelated natural and synthetic compounds that inhibit microtubule polymerization bind to the colchicine-binding site of tubulin (*26*, *28*, *29*). Like colchicine, menadione also inhibited tubulin polymerization. Thus, we examined whether menadione binds at the colchicine binding site of tubulin. Colchicine does not fluoresce in aqueous solution, but it fluoresces when it binds to tubulin (*47*). Tubulin was incubated with a fixed concentration of colchicine and different concentrations of menadione (0–80 μM), and the fluorescence of colchicine of different samples was measured at 430 nm while the excitation wavelength was 380 nm which selectively excited only colchicine but not menadione. Although absorption spectra of menadione and colchicine have some overlap, the extinction coefficient of menadione at 380 nm (862 M^{-1} cm^{-1}) is very low compared to that of colchicine at 380 nm (7060 M^{-1} cm^{-1}). We also checked the fluorescence values of tubulin and menadione complexes at 430 nm after excitation at 380 nm and found them to be very low, and those values were subtracted from those of the corresponding tubulin–menadione–colchicine complex. Menadione inhibited binding of colchicine to tubulin in a concentration-dependent manner. The data were analyzed using a modified Dixon plot (Figure 11A). The results clearly indicate that binding of menadione to tubulin was inhibited competitively by colchicine, yielding a K_i value of 2.5 μM. One of the important characteristics of colchicine binding to tubulin is its irreversibility. This property of drug–protein interaction has been found to be a property of colchicine structure and its B-ring side chain. Here, we present interesting data for an inhibitor that is structurally unrelated to colchicine but bears important similarity with the colchicine–tubulin interaction. To determine whether binding of menadione to tubulin occurs in a reversible mode, we incubated menadione (15 μM) with tubulin (3 μM) at 25 °C. At different time intervals, the drug–protein complex was withdrawn and the extent of free

colchicine binding of tubulin was estimated using a colchicine analogue without B-ring AC [2-methoxy-5-(2′,3′,4′-trimethoxyphenyl)tropone], which binds tubulin instantaneously at the colchicine site and gives fluorescence at 430 nm (*28*). Results of such an experiment where fluorescence of AC was measured at 430 nm are shown in Figure 11B. The results indicate that the fluorescence value of AC decreases with an increase in the incubation time of the tubulin−menadione complex at 25 °C. Here the fluorescence of the AC−tubulin complex without menadione was taken to be 100% (control), and the fluorescence of the tubulin−menadione complex incubated for 10 min at 25 °C was found to be 28% less than the control value. The fluorescence of the complex decreases further to 52% when the complex is incubated for 45 min. Under this identical condition, menadione binds ∼78% (based on the calculation considering a K_d of 3.65 μM for the tubulin−menadione complex) of the total tubulin present in incubation mixture. Therefore, this data clearly indicate that the interaction of menadione with tubulin is not reversible in nature. These data are corroborated by irreversible depolymerization of microtubules in HeLa cells by menadione.

DISCUSSION

Vitamin K3 cancer research has focused on two basic mechanisms to explain these effects. The older mechanism relies on an oxidative effect produced by the one-electron cycling of vitamin K3 that surpasses the oxidative capacity of the cancer cell, leading to death (*9*). The latest research on vitamin K3 has led researchers to discover an alternative anticancer mechanism of action that acts at the level of protein kinases and phosphatases (*18*). Vitamin K3 has been found to act on proteins such as c-myc and c-fos (*48*), as it can promote both proliferation and apoptosis depending on its expression. Cell cycle arrest has also been found to be initiated by phosphatases at the level of cyclins, which are critical in the cell cycle (*48*). A variety of inhibitors of ABC drug transporters have been developed to date with the objective of reversing resistance against anticancer drugs and chemosensitizing the resistant cells to anticancer drugs. The fact that vitamin K3 can inhibit the ABCG2-mediated function suggests that these types of compounds can be developed as inhibitors of this transporter to overcome ABCG2-mediated multidrug resistance (*49*).

Although menadione is a potential anticancer agent, there is no direct evidence of its target site inside the cell. The novel results of this study are that menadione inhibited tubulin polymerization

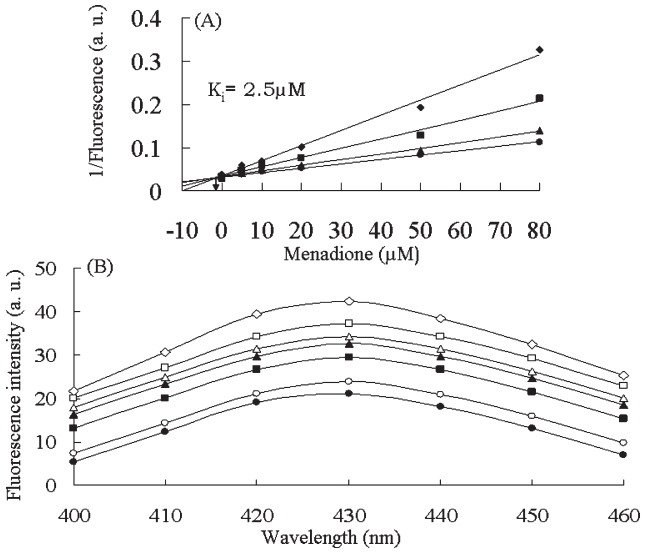

FIGURE 11: Menadione inhibited the binding of colchicine to tubulin. (A) Modified Dixon plot. The concentrations of colchicine were 5 (◆), 7.5 (■), 10 (▲), and 15 μM (●). The reaction mixture contained tubulin (3 μM) and menadione at the indicated concentration (0−75 μM), and the mixture was incubated at 37 °C for 1 h. Data are represented as means ± SEM ($p < 0.01$) where $n = 3$. (B) Reversible binding study. Tubulin at 3 μM was incubated with menadione (15 μM) for different periods of time [0 (◇), 5 (□), 10 (△), 20 (◇), 30 (■), and 60 min (●)], and then 30 μM AC was added to the sample separately. Fluorescence spectra were recorded when the excitation wavelength was 370 nm.

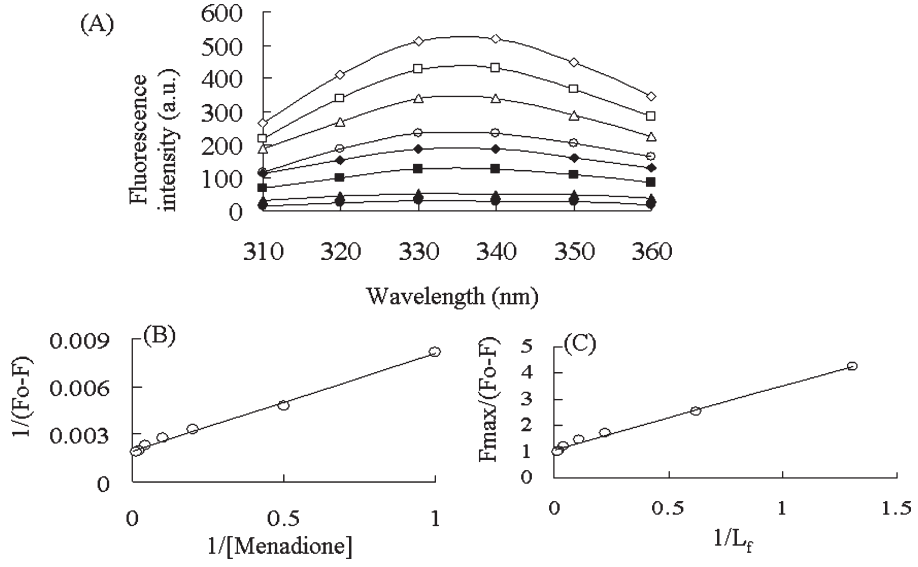

FIGURE 10: Characterization of binding of menadione to tubulin using quenching of tryptophan residues of tubulin. (A) Menadione [1 (□), 2 (△), 5 (◇), 10 (◆), 25 (■), 50 (▲), and 75 μM (●)] reduced the intrinsic tryptophan fluorescence of tubulin (2 μM) with respect to tubulin fluorescence (◇) in the absence of menadione. The excitation wavelength was 295 nm. The inset shows the percentage of tryptophan quenching at different menadione concentrations. (B) Double-reciprocal plot of menadione binding to tubulin. F_{max} has been determined from the $1/(F_0 - F)$ and 1/[menadione] graph. (C) Linear plot of binding of menadione to tubulin. Data are represented as means ± SEM ($p < 0.01$) where $n = 3$. Data are representative of three identical experiments.

in microtubules in vitro and significantly bound to the purified tubulin. On the basis of the strong effects of menadione on tubulin and microtubules in vitro, we also examined whether menadione inhibited the proliferation of HeLa cells with an IC_{50} of ≈26 μM and KB (human nasopharyngeal epithelial carcinoma cell) cells with an IC_{50} of ≈63 μM; both cell lines express high levels of P-glycoprotein and show resistance to a number of anticancer drugs. Menadione significantly induced apoptosis in the HeLa cells and also blocked the cell cycle at G2/M phase and arrest at mitosis. Menadione depolymerized the interphase microtubule and also disrupted the spindle assembly of the mitotic cells. It showed an irreversible pattern of cellular damage unlike vinblastine and colcemid (*45*) but like cryptophycin (*46*) and sanguinarin (*47*). Cells treated with menadione remained depleted of microtubules for at least 24 h after the compound was removed from the cultures. This irreversible damage pattern of menadione may be due to irreversible loss of activity of tubulin polymerization-promoting factors by denaturation and/or proteolysis or irreversible damage of their binding pocket to tubulin. These actions on mammalian cell tubulin and microtubules suggest that the inhibition of cancer cell proliferation by menadione in humans may be due in part to the perturbation of microtubule function. We found that menadione inhibits the polymerization of mammalian brain tubulin, with 50% inhibition (IC_{50}) of polymerization occurring at a menadione concentration of 46 μM. Thus, its ability to inhibit microtubule polymerization is significant. The association of menadione with the purified tubulin is biphasic in nature like that of colchicine, with rate constants of 111.35 ± 24 and $72.61 \pm 11\ M^{-1}\ s^{-1}$ for the fast and slow phases, respectively. We have also shown that menadione binds at the colchicine binding site of the tubulin with a significant K_i value of 2.5 μM. Like that of colchicine, the biphasic nature of the menadione−tubulin interaction arises perhaps due to the differential binding property of menadione to β-tubulin isotypes present in brain tubulin. We have used ligand as well as protein fluorescence to determine the binding affinity of menadione for mammalian brain tubulin. Using enhancement of ligand fluorescence upon binding with tubulin at 418 nm, we obtained a K_d of 3.65 ± 0.25 μM, whereas using quenching of protein fluorescence, we obtained a K_d of 2.44 ± 0.34 μM. Thus, the affinity of menadione for brain tubulin is strong and robust. Colchicine binds to tubulin with high affinity ($K_d = 0.1-0.5$ μM). Interestingly, high concentrations of menadione were required to inhibit microtubule polymerization ($IC_{50} = 46$ μM), whereas its affinity (K_d) for tubulin was ≈2.44−3.65 μM. Thus, menadione probably does not inhibit microtubule polymerization through a simple end poisoning mechanism like that which occurs with colchicine and vinblastine.

In contrast to vitamin K3, phylloquinone (vitamin K1), which is present naturally in green leafy vegetables and catabolized to vitamin K3 inside the body, neither exhibits cytotoxicity against HeLa cells nor disrupts the microtubule network in HeLa cells; it even does not inhibit tubulin polymerization in vitro (data not shown). Although the orally absorbed phylloquinone is strongly catabolized to the menadione by 5−25% (*7*), dietary phylloquinone will be more than enough as menadione supplements inside the body. In January 2001, The Food and Nutrition Board (FNB) of the Institute of Medicine established the adequate intake (AI) levels for vitamin K in U.S. adults are 120 μg/day (in men) and 90 μg/day (in women). In an advanced malignancy phase I trial of menadione given as a rapid intravenous infusion, patients were able to tolerate dose levels from 40 to 200 mg/m^2 with no hematological toxicity, although some grade I and grade II hypersensitivity reactions occurred at the highest dose of 1360 mg/m^2, but no dose-limiting organ system toxicity was observed (*50*). This suggests that perhaps a longer infusion of menadione would achieve the peak drug level which has already been demonstrated to be cytotoxic for sensitive malignant cell lines.

In summary, the antiproliferative activity of menadione has been correlated to its ability to perturb microtubule networks through tubulin binding at the colchicine site. Nature has presented us the tubulin microtubule as a highly successful anticancer target. Many natural compounds that target the tubulin−microtubule system are in different stages of drug development. Thus, menadione alone or in combination with other antimicrotubule agents may be evaluated for its clinical potential against several types of cancers.

ACKNOWLEDGMENT

We thank Prof. Bhabatarak Bhattacharyya (Department of Biochemistry, Bose Institute, Kolkata, India) for suggestions during the course of the work. Confocal Microscope and FACS facilities were provided by a grant from the National Common Minimum Program, Government of India.

REFERENCES

1. Esmon, C. T., Suttie, J. W., and Jackson, C. M. (1975) The functional significance of vitamin K action. Difference in phospholipid binding between normal and abnormal prothrombin. *J. Biol. Chem. 250*, 4095–4099.
2. Tuan, R. S. (1979) Vitamin K-dependent γ-glutamyl carboxylase activity in the chick embryonic chorioallantoic membrane. *J. Biol. Chem. 254*, 1356–1364.
3. Mijares, M. E., Nagy, E., Guerrero, B., and Arocha-Pinango, C. L. (1998) Vitamin K: Biochemistry, function, and deficiency. *Rev. Invest. Clin. 39*, 213–229.
4. Li, Z. Q., He, F. Y., Stehle, C. J., Wang, Z., Kar, S., Finn, F. M., and Carr, B. I. (2002) Vitamin K uptake in hepatocytes and hepatoma cells. *Life Sci. 70*, 2085–2100.
5. Thomson, R. H. (1971) Naturally Occurring Quinones , Academic Press, New York.
6. Conley, J. M., and Stein, K. (1992) The production of menaquinones (vitamin K2) by intestinal bacteria and their role in maintaining coagulation homeostasis. *Prog. Food Nutr. Sci. 16*, 307–343.
7. Henk, H., Thijssen, W., Lily, M. T., Vervoort, L., Schurgers, J., and Martin, J. S (2006) Menadione is a metabolite of oral vitamin K. *Br. J. Nutr. 95*, 260–266.
8. Mitchell, J. S., and Simon-Reuss, I. (1947) Combination of some effects of X-radiation and a synthetic vitamin K substitute. *Nature 160*, 98–99.
9. Lamson, D. W., and Plaza, S. M. (2003) The anticancer effects of vitamin K. *Altern. Med. Rev. 8*, 303–318.
10. Prasad, K. N., Edwards-Prasad, J., and Sakamoto, A. (1981) Vitamin K3 (menadione) inhibits the growth of mammalian tumor cells in culture. *Life Sci. 29*, 1387–1392.
11. Gold, J. (1986) In vivo synergy of vitamin K3 and methotrexate in tumor-bearing animals. *Cancer Treat. Rep. 70*, 1433–1435.
12. Chlebowski, R. T., Dietrich, M., Akman, S., and Block, J. B. (1985) Vitamin K3 inhibition of malignant murine cell growth and human tumor colony formation. *Cancer Treat. Rep. 69*, 527–532.
13. Ngo, E. O., Sun, T. P., and Chang, J. Y. (1991) Menadione induced DNA damage in a human tumor cell line. *Biochem. Pharmacol. 42*, 1961–1968.
14. Su, W. C., Sun, T. P., and Wu, F. Y. (1991) The *in vitro* and *in vivo* cytotoxicity of menadione (vitamin K3) against rat transplantable hepatoma induced by 3′-methyl-4-dimethyl-aminoazobenzene. *Gaoxiong Yi Xue Ke Xue Za Zhi 7*, 454–459.
15. Nutter, L. M., Cheng, A. L., and Hung, H. L. (1991) Menadione: Spectrum of anticancer activity and effects on nucleotide metabolism in human neoplastic cell lines. *Biochem. Pharmacol. 41*, 1283–1292.
16. Kerns, J., Naganathan, S., Dowd, P., Finn, F. M., and Carr, B. (1988) Thioalkyl Derivatives of Vitamin K3 and Vitamin K3 Oxide Inhibit Growth of Hep3B and HepG2 Cells. *Chem.-Biol. Interact. 65*, 157–173.

17. Naohiro, S., Hanne, K. S., Bing, H., Dieter, H., and Claus, N. (1997) Menadione Induces Both Necrosis and Apoptosis in Rat Pancreatic Acinar AR4-2J Cells. *Free Radical Biol. Med. 23*, 844–850.
18. Markovits, J., Wang, Z., Carr, B. I., Sun, T. P., Mintz, P., Le Bret, M., Wu, C. W., and Wu, F. Y. (2003) Differential effects of two growth inhibitory K vitamin analogs on cell cycle regulating proteins in human hepatoma cells. *Life Sci. 72*, 2769–2784.
19. Tamura, K., Southwick, E. C., Kerns, J., Rosi, K., Carr, B. I., Wilcox, C., and Lazo, J. S. (2000) Cdc25 Inhibition and Cell Cycle Arrest by a Synthetic Thioalkyl Vitamin K Analogue. *Cancer Res. 60*, 1317–1325.
20. Sumio, M., Yuka, Y., Takeshi, A., Toshikatsu, N., and Kenji, M. (2008) An Attempt to Evaluate the Effect of Vitamin K3 Using as an Enhancer of Anticancer Agents. *Biol. Pharm. Bull. 31*, 1270–1273.
21. Lodish, H., Baltimore, D., Berk, A., Zipursky, S. L., Matsudaira, P., and Darnell, J. (1999) Molecular and Cellular Biology , W. H. Freeman, New York.
22. Nogales, E., Wolf, S. G., and Downing, K. H. (1998) Structure of the $\alpha\beta$ tubulin dimer by electron crystallography. *Nature 391*, 199–203.
23. Downing, K. H., and Nogales, E. (1998) Tubulin and microtubule structure. *Curr. Opin. Cell Biol. 10*, 16–22.
24. Kirschner, M., and Mitchison, T. (1986) Beyond self-assembly: From microtubules to morphogenesis. *Cell 45*, 329–342.
25. Desai, A., and Mitchison, T. J. (1997) Microtubule polymerization dynamics. *Annu. Rev. Cell Biol. 13*, 83–117.
26. Jordan, M. A., and Wilson, L. (2004) Mechanism of action of antitumor drugs that interact with microtubules and tubulin. *Nat. Rev. Cancer 4*, 253–265.
27. Kumar, N. (1981) Taxol induced polymerization of purified tubulin, mechanism of action. *J. Biol. Chem. 256*, 10435–10441.
28. Acharya, B. R., Bhattacharyya, B., and Chakrabarti, G. (2008) The natural naphthoquinone plumbagin exhibits antiproliferative activity and disrupts the microtubule network through tubulin binding. *Biochemistry 47*, 7838–7845.
29. Bhattacharyya, B., Panda, D., Gupta, S., and Banerjee, M. (2008) Anti-mitotic activity of colchicine and the structural basis for its interaction with tubulin. *Med. Res. Rev. 28* (1), 155–183.
30. Uppuluri, S., Knipling, L., Sackett, D. L., and Wolff, J. (1993) Localization of the colchicine-binding site of tubulin. *Proc. Natl. Acad. Sci. U.S.A. 90*, 11598–11602.
31. Rai, S. S., and Wolff, J. (1996) Localization of the vinblastine binding site on β-tubulin. *J. Biol. Chem. 271*, 14707–14711.
32. Kamath, K., and Jordon, M. A. (2003) Suppression of microtubule dynamics by Epothilone B is associated with mitotic arrest. *Cancer Res. 63*, 6026–6031.
33. Minnoti, A. M., Barlow, S. B., and Cabral, F. (1991) Resistance to antimitotic drugs in chinese hamster ovary cells correlates with changes in the level of polymerized tubulin. *J. Cell Biochem. 266*, 3987–3994.
34. Hamel, E., and Lin, C. M. (1981) Glutamate-induced polymerization of tubulin: Characteristics of the reaction and application to the large-scale purification of tubulin. *Arch. Biochem. Biophys. 209*, 29–40.
35. Bradford, M. M. (1976) A rapid and sensitive method for the quantitation of microgram quantities of protein utilizing the principle of protein-dye binding. *Anal. Biochem. 72*, 248–254.
36. Vanoni, A. M., Ballou, D. P., and Matthews, G. R. (1983) Methylene-tetrahydrofolate reductase, stady state and rapid reaction studies on the NADPH-methylenetetrahydrofolate, NADPH-menadione and methyltetrahydrofolate-menadione oxidoreductase activities of the enzyme. *J. Biol. Chem. 258*, 11510–11514.
37. Gaskin, F., Cantor, C. R., and Shelanski, M. L. (1974) Turbidimetric studies of the in vitro assembly and disassembly of porcine neurotubules. *J. Mol. Biol. 89*, 737–755.
38. Lakowicz, J. R. (1999) Principles of Fluorescence Spectroscopy , 2nd ed., Kluwer Academic/Plenum Publishers, New York.
39. Chakrabarti, G., Sengupta, G., and Bhattacharyya, G. (1996) Thermodynamics of Colchicinoid-Tubulin Interactions: Role of B ring and C7 substituent. *J. Biol. Chem. 271*, 2897–2901.
40. Lambeir, A., and Engelborghs, Y. (1981) A fluorescence stopped flow study of colchicine binding to tubulin. *J. Biol. Chem. 256*, 3279–3282.
41. Wang, J. L., and Edelman, G. M. (1971) Fluorescent probes for conformational states of proteins. IV. The pepsinogen−pepsin conversion. *J. Biol. Chem. 246*, 1185–1191.
42. Ward, L. D. (1985) Measurement of ligand binding to protein by fluorescence spectroscopy. *Methods Enzymol. 117*, 400–414.
43. Bhattacharyya, B., and Wolff, J. (1974) Promotion of fluorescence upon binding of colchicine to tubulin. *Proc. Natl. Acad. Sci. U.S.A. 71*, 2627–2631.
44. Chakraborty, S., Gupta, S., and Bhattacharyya, B. (2004) The B-ring substituent at C-7 of colchicine and the R-C-terminus of tubulin communicate through the "tail-body". *Proteins 57* (3), 602–609.
45. Manley, M., and Brinkley, B. R. (1972) Mitosis in Human Leukemic Leukocytes during Colcemid Inhibition and Recovery. *Cancer Res. 32*, 746–755.
46. Smith, D. C., Zhang, X., Mooberry, S. L., and Moore, R. E. (1994) Cryptophycin: A new antimicrotubule agent active against drug-resistant cells. *Cancer Res. 54*, 3779–3784.
47. Lopus, M., and Panda, D. (2006) The benzophenanthridine alkaloid sanguinarine perturbs microtubule assembly dynamics through tubulin binding A possible mechanism for its antiproliferative activity. *FEBS J. 273*, 2139–2150.
48. Wu, F. Y., Chang, N. T., Chen, W. J., and Juan, C. C. (1993) Vitamin K3-induced cell cycle arrest and apoptotic cell death are accompanied by altered expression of c-fos and c-myc in nasopharyngeal carcinoma cells. *Oncogene 8*, 2237–2244.
49. Shukla, S., Chung, P. W., Nandigama, K., and Ambudkar, S. V. (2007) The naphthoquinones, vitamin K3 and its structural analogue plumbagin, are substrates of the multidrug resistance-linked ATP binding cassette drug transporter ABCG2. *Mol. Cancer Ther. 6* (12), 3279–3286.
50. Lim, D., Morgan, R. J., and Doroshow, J. H. (2005) Phase I trial of menadiol diphosphate (vitamin K3) in advanced malignancy. *Invest. New Drugs 23*, 235–239.